ELSEVIER

Journal of Nuclear Materials 290–293 (2001) 633–638

journal of nuclear materials

www.elsevier.nl/locate/jnucmat

Observation of detachment in the JET MkIIGB divertor using CCD camera tomography

K. Itami [b,*], P. Coad [a], W. Fundamenski [a], C. Ingesson [a], J. Lingertat [a], G.F. Matthews [a], A. Tabasso [a]

[a] *JET Joint Undertaking, Abingdon, Oxfordshire, OX14 3EA, UK*

[b] *Japan Atomic Energy Research Institute (JAERI), Naka-Site, 801 Mukoyama, Naka-machi, Naka-gun, Ibaraki-ken 311-0193, Japan*

Abstract

In this paper, we discuss Dα and Dγ profiles in a density limit discharge in L-mode. CCD camera tomography was developed, calibrated with KS3 visible spectroscopy and utilized to observe two-dimensional change in Dα and Dγ profiles. A significant difference in Dα profiles was found between the inner and outer divertor. While the Dα profile extended to fill the inner divertor as the plasma density increased, in the outer divertor the Dα profile extended along the separatrix. From the comparison of Dα and Dγ profiles along the separatrix, it was found that recombination became significant and the recycling peak shifted upstream before full detachment of both the inner and outer divertor.

Keywords: Dα line; CCD camera Tomography; Divertor detachment

1. Introduction

Through a study of Dγ/Dα line ratios in the JET MkIIa divertor, volume recombination was shown to play an important role in detachment [1]. During the subsequent period of JET operation with the more closed MkIIGB divertor, a tangentially viewing endoscope system was installed which views the X-point region at three wavelengths (Dα, Dγ and CII lines) simultaneously. In this paper, results are presented from tomographic reconstruction of these views which show the evolution of the 2D distributions of Dα and Dγ during detachment.

2. Alignment of the endoscope optics to Dα and Dγ video images

Accurate identification of the CCD camera view through endoscope optics is crucially important for CCD camera tomography calculations. The three-dimensional (3D) structure of the MkIIGB divertor was modeled and projected to the view plane which is perpendicular to the optical axis Fig. 1. This projection simulates the video image of the divertor structure. The projection is measured in video pixels. Orientation of the optical axis, view angle and rotation of image must be determined to simulate the video image of the CCD camera. In addition to those geometrical parameters, vertical and horizontal offsets of the video images must be corrected so that the center of the video image coincides with the optical axis in the software. Bright images of the disruptive discharge were used to identify tile gaps and the silhouette of divertor structure in both Dα and Dγ filtered images. All of the above parameters were determined iteratively so that tile gaps and the silhouette of divertor structure in the simulated video images could be overlapped with those in the real video image.

In the process of identification of Dα and Dγ camera views, pixel maps of Dα and Dγ images were created. A series of beam splitters was used at the output of the endoscope to observe three wavelength simultaneously. Therefore, the Dα and Dγ camera

* Corresponding author. Tel.: +81-29 270 7343; fax: +81-29 270 7419.

E-mail address: itamik@fusion.naka.jaeri.go.jp (K. Itami).

0022-3115/01/$ - see front matter
PII: S0022-3115(00)00520-1

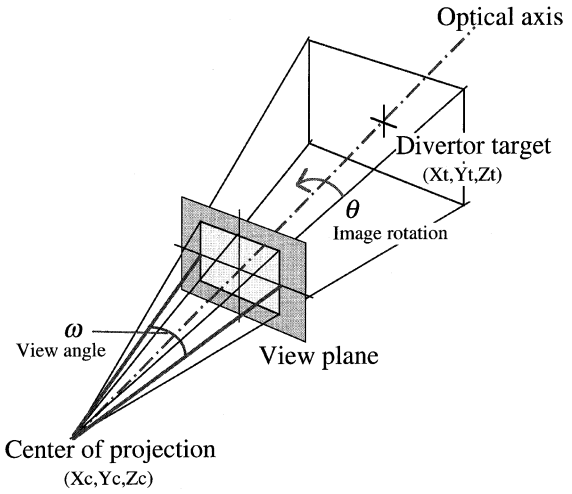

Fig. 1. Schematic view of the projection to the view plane in the 3D view computing program and the parameters to change for identification of the Dα and Dγ camera views. The center of projection is the entrance pupil of the endoscope, and its position is fixed.

alignment was found to be very similar. These pixel maps link each video pixel to a 3D coordinate on the divertor tile. These maps were used to create the inversion (geometry) matrix in the tomographic calculation.

Twenty-five video frames were recorded per second. A video frame consisted of two interlaced video fields in which the time code was stamped. Since the video frame grabber hardware can capture each video field, the time resolution of the Dα and Dγ images was 20 ms.

3. CCD camera tomography

Tomography is a technique used to calculate local emissivity profiles from the line-integrated value along the detector. CCD camera tomography [2–4] utilizes data from a large number of video pixels to calculate emissivities on the two-dimensional (2D) grid in the divertor by assuming toroidal symmetry. Figs. 2(a) and (b) show the video grids and divertor grids which are used in this paper.

The tomographic inversion is reduced to a problem of solving the linear equations,

$$[A][x] = [b]. \tag{1}$$

Here, $[x]$ is a vector of emissivity on the divertor grids. $[b]$ is signal intensity on the video pixel. $[A]$ is the geometry matrix, of which elements are chord integrals of Dα and Dγ line emissivities from the divertor structure to the CCD camera. In this paper, we call 'inversion' the calculation to obtain an approximate solution [x_s] in Eq. (1) and call 'reconstruction' the reconstruction of video image $[b\_s] = [A][x\_s]$. Element (i, j) of the geometry matrix is the line length inside the jth divertor grid along the chord which starts from the position mapped to the ith video grid and ends at the center of the projection. The matrix is completed by repeating for all video grids. The inversion matrix is sparse. Typically less than 10% of the elements is filled.

Singular value decomposition (SVD) [5] decomposes matrix $[A]$ into

$$[A] = [U][w][V^{\mathrm{T}}]. \tag{2}$$

Here, M is the number of the video grid and N is the number of the divertor grid in CCD camera tomography. $[U]$ is a $M \times N$ column orthogonal matrix, $[V^{\mathrm{T}}]$ is the transpose of an $N \times N$ orthogonal matrix. $[w]$ is an $N \times N$ diagonal matrix with positive or zero elements and the matrix represents the singularity of matrix $[A]$. $M > N$ is satisfied. When $M > N$, the solution of Eq. (1) in the least square sense, minimizing $|[A][x\_s] - [b]|$, is given by

$$[x\_s] = [V][1/w][U^{\mathrm{T}}][b]. \tag{3}$$

Here, $[1/w]$ is basically the inverse of the $N \times N$ diagonal matrix. However, zero elements and small value elements are removed. The tolerance (TOL), $w_{i\,\min}/w_{i\,\max}$, defines the minimum w_i in $[1/w]$. $TOL = 0.05$ was empirically used so that the Dα and Dγ profiles were smooth both in space and time.

The solution obtained by SVD contains negative values. Negative values were redistributed iteratively until the absolute value of the negative values was less than one-fifth of the maximum. In iteration, negative elements of the solution were used to reconstruct a virtual negative image. This negative image was inverted by SVD; however, the divertor grids of the negative elements were removed from the calculation. A solution in the iteration was obtained by adding the solution of the negative image to the positive element of the previous solution, while negative elements in the previous solution were set to zero. The final solutions were reconstructed and compared with original video data. While fine structures including noises were lost, overall features in the video images were restored.

4. Experimental results

Time evolution of Dα and Dγ profiles by the CCD tomography technique was analyzed in a density

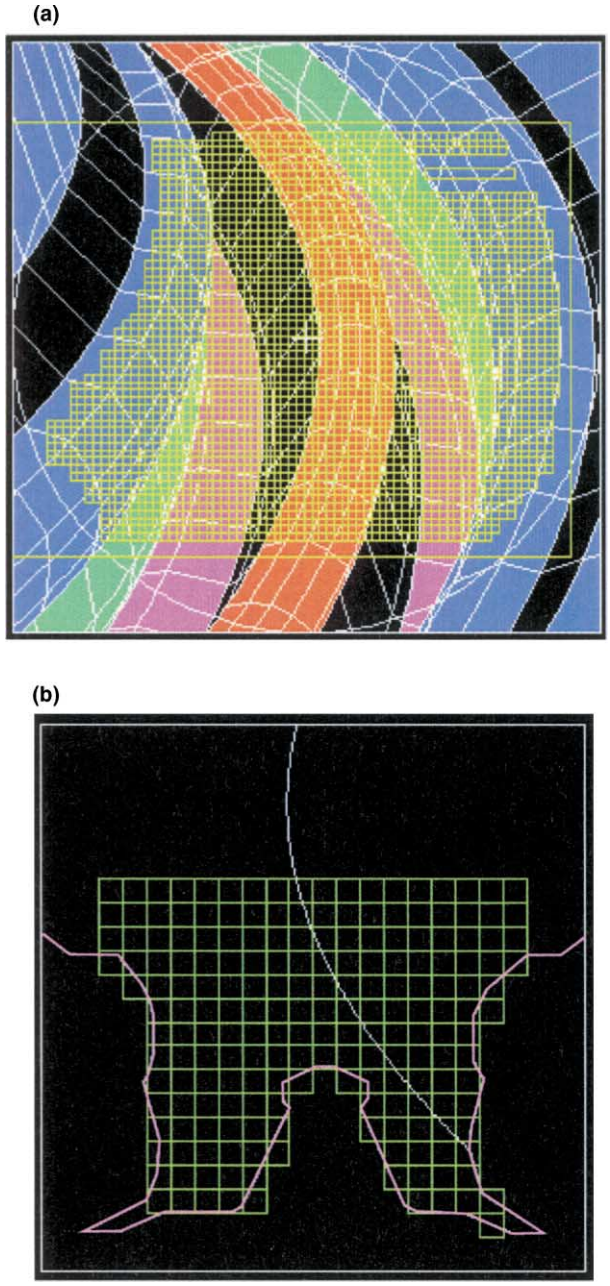

Fig. 2. (a) A simulated view of the MkIIGB divertor structure shown with the video grids for CCD camera tomography. The top of the septum is drawn in red, the upper wall targets in blue, the lower wall targets in green, the divertor floor in pink. (b) A cross-section of the MkIIGB divertor structure shown with the video grids and divertor grids for CCD camera tomography. The curved line is an example of a trajectory from the divertor to a video pixel mapped to a poloidal plane.

limit discharge. The plasma density was increased, as shown in Fig. 3(a), gradually by gas puffing in an L-mode discharge with a plasma current of 2 MA, toroidal field of 2.4 T and beam heating power of 2 MW.

Dα and Dγ profiles from CCD camera tomography were calibrated with the KS3 system. KS3 is a visible survey spectrometer. KS3I and KS3O provide integrated Dα and Dγ signals over the inner divertor and the outer divertor, respectively. In order to simulate

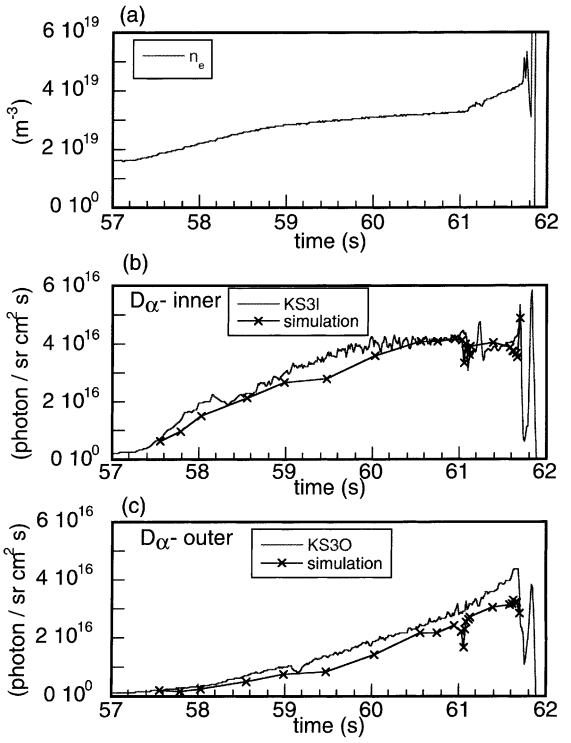

Fig. 3. (a) Volume-averaged plasma density time trace; (b) Dα intensity on the KS3I system shown with simulated KS3I data; (c) Dα intensity on the KS3O system shown with simulated KS3O data.

KS3I and KS3O data, Dα and Dγ profiles were integrated along the same chord and averaged over the same radial extent with KS3I and KS3O, respectively. The calibration factors were determined so that the simulated KS3I data matched the measured KS3I data at $t = 60.5$ s in the density limit discharge of Fig. 3. The waveforms of the KS3I and KS3O data and the simulated data are shown in Fig. 3(b) and (c). The time resolution of the KS3I and KS3O data is 20 ms. X-marks in these figures are the selected times when the calculation of the line integral was done from the inversion images. As shown in these figures, the difference between the measured data and simulation is small even though the signal amplitude increases an order of magnitude over the time shown. Some deviation is seen at $t = 59.5$ s, probably due to noise in the video image. The simulated Dα data of the outer divertor was ~10% lower than the measured KS3O data. For Dγ data, the difference between the measured KS3I and KS3O data and simulation data is small in both divertors except during the full detachment of the inner divertor.

The time evolution of the Dα profile is shown in Fig. 4. The maximum scale in these plots is 1.9×10^{23} photon/m^3 s. In the early phase, the Dα intensity rapidly increased as the plasma density went up to $n_e \sim 2.7 \times 10^{19}$ m^{-3} at $t = 58.55$ s. The Dα profile peaked on the inner target wall. The Dα intensity on the inner target reached a maximum value and then gradually decreased after $t = 58.55$ s, while the Dα profile extended upward and radially. The ion saturation current (I_{sat}) of the divertor Langmuir probes near the inner strike point rolled over, indicating that the plasma was detaching in the inner divertor. However, Dα increased linearly at the outer divertor and I_{sat} at the outer strike point also increased until full detachment of the inner divertor. While the Dα profile extended two-dimensionally in the inner divertor, the Dα profile extended along the outer leg separatrix. After $t = 60.03$ s, the upstream Dα intensity increased strongly and the Dα profile filled the inner divertor region. At $t = 60.55$ s the upstream Dα intensity dominated that on the inner target. A drastic change in the Dα profile happened with the full detachment of the inner divertor, which started at $t = 61.03$ s. The local peak of Dα intensity (Dα blob) took off from the inner target and jumped to midway between the target and the X-point within the time of four video fields, i.e., within 80 ms. The Dα intensity on the target vanished with this fast movement of the Dα blob. This full detachment of the inner divertor was observed as a sudden drop in Dα intensity of both KS3I and the simulation. This sudden drop was caused by a decrease in the peak Dα intensity in the blob during the jump. The sudden drop in the intensity was also found in the Dα intensity at the outer divertor. Dα intensity at the outer divertor increased again after $t = 61.11$ s, while the intensity and the local Dα profile did not change at the inner divertor. Divertor Langmuir probe measurement showed that the outer divertor was detaching.

In order to investigate divertor detachment more precisely, we studied the Dα and Dγ profiles along the separatrix. For this purpose, the solution cell was defined as shown in Fig. 5(a). Two vertical divertor grids across the separatrix constitute a solution cell. Dα and Dγ intensity was averaged in the cell. As shown in Fig. 5(b) and (c), Dγ is more peaked near the divertor target. As the density increased upstream the Dα and Dγ intensity increased. After $t = 60.03$ s, the Dα intensity peak shifted upstream. On the other hand, the change in Dγ profile was mild and Dγ had a peak on the target until full detachment occurred.

In the outer divertor no significant change in the Dα and Dγ profile was observed before the full de-

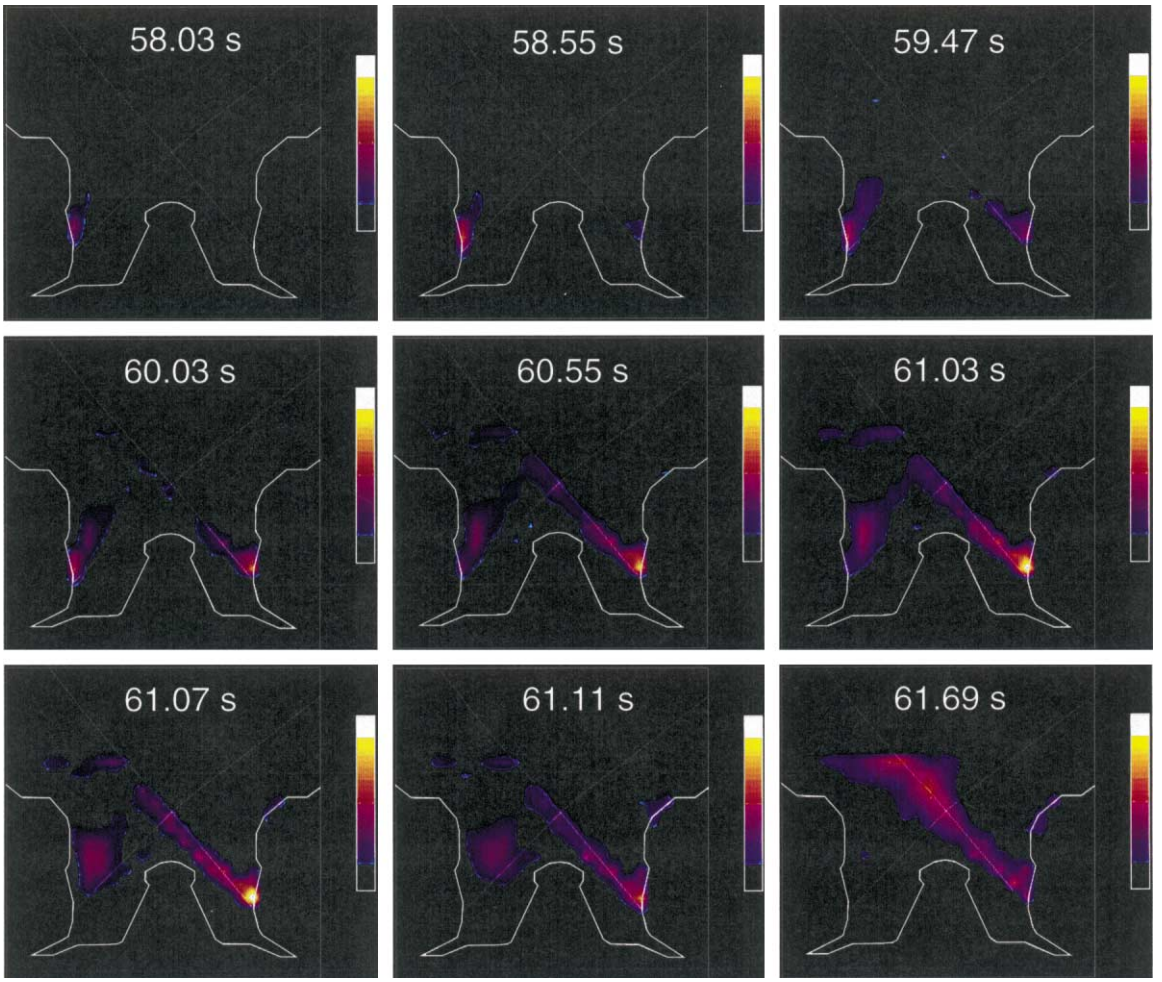

Fig. 4. Time evolution of Dα profiles by CCD camera tomography. The color bar is a linear scale of intensity: the bottom of the black region is 0 photon/m^3 and top of the white region is 1.9×10^{23} photon/m^3 s.

tachment of the inner divertor, while the Dγ profile was more peaked than the Dα profile along the outer leg separatrix near the strike point. After the full detachment of the outer divertor, a similar change in Dα and Dγ profiles to those in the inner divertor was observed.

Fig. 6(a) shows the Dγ/Dα ratio in the grids on the inner target, and Fig. 6(b) shows the ion flux measured by the divertor Langmuir probes. The probe data indicate that the divertor detachment was spreading over the divertor target. After $t = 60$ s, the Dγ/Dα ratio increased from 0.04 to 0.08 in a divertor grid on the inner target just before the inner divertor plasma fully detached. Therefore, the full detachment of the inner divertor was accompanied by strong recombination [3,4,6] near the divertor target.

5. Summary

CCD tomography, which calculates two-dimensional Dα and Dγ profiles with a time resolution of 20 ms, was developed for the observation of detachment of the JET MkIIGB divertor. Cross-calibration was done with the KS3 system for both Dα and Dγ signals.

Significant difference in Dα profiles was observed between the inner and outer divertor. Dα profiles in the inner divertor extended vertically and radially from the target, while Dα profiles in the outer divertor extended along the field line in the outer leg, as the plasma density increased.

Analysis of Dα and Dγ emissivity profiles along the field line showed that the recycling front gradually

shifted from the target upstream as the volume recombination significantly increased prior to full detachment of the inner divertor.

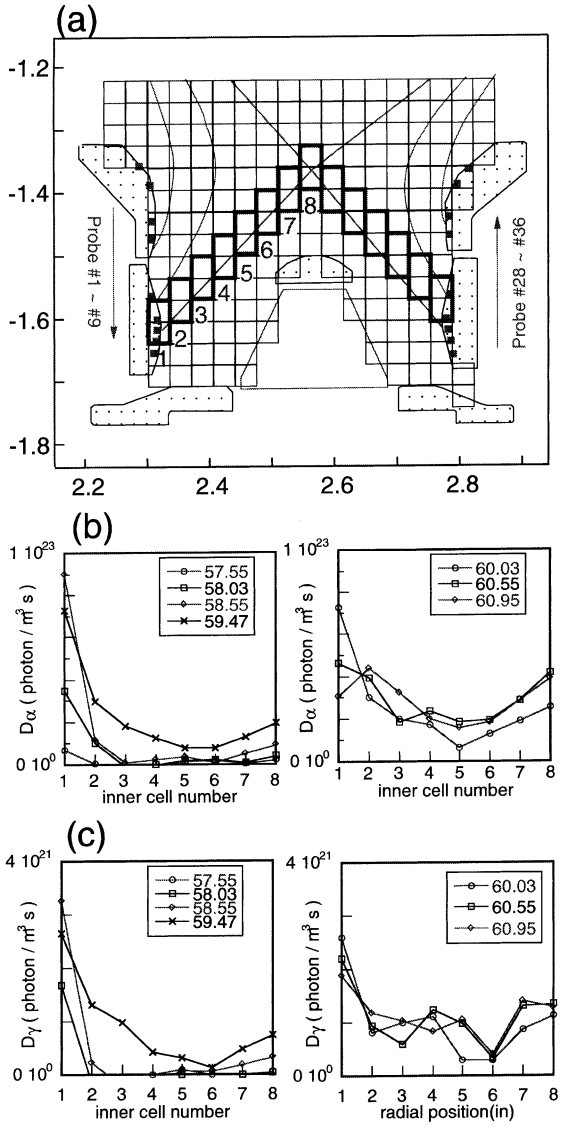

Fig. 5. (a) Divertor grids and location of the solution cells along the separatrix. The inner cell #1 is located at the target and the inner cell #8 is located at the X-point. (b) Time evolution of Dα profile along the separatrix of the inner leg. (c) Time evolution of Dγ profile along the separatrix of the inner leg.

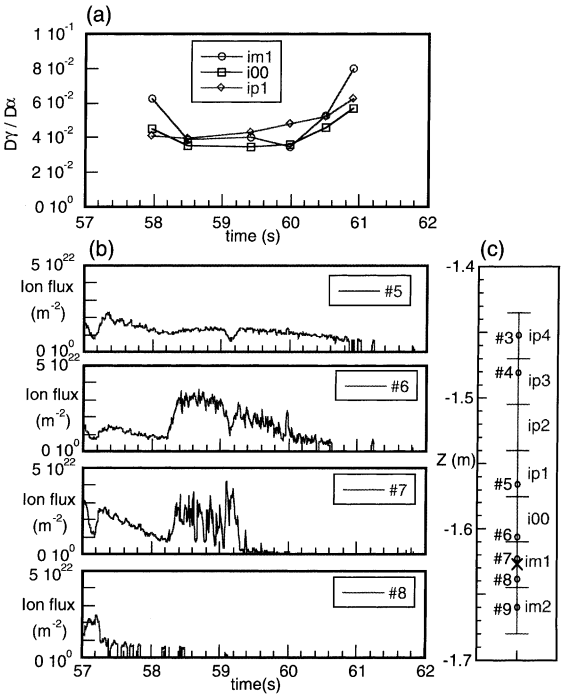

Fig. 6. (a) Time traces of Dγ/Dα ratio in the grids on the inner target. Vertical positions of the divertor grids are indicated in (c). (b) Ion flux measured by the divertor Langmuir probes. Vertical positions of the probes are indicated in (c). (c) Divertor probe positions are shown with divertor grids on the inner target, which are lined vertically. The strike point position is marked by X.

References

[1] G. McCracken et al., J. Nucl. Mater. 266–269 (1999) 37.
[2] M.E. Fenstermacher et al., Rev. Sci. Instrum. 68 (1) (1997) 974.
[3] M.E. Fenstermacher et al., J. Nucl. Mater. 266–269 (1999) 348.
[4] C. Boswell, J.L. Terry, B. Lipschults, Bull. Am. Phys. Soc. 43 (8) (1998) 1823.
[5] M. Anton et al., Plasma Phys. Controlled Fus. 38 (1996) 1849.
[6] H. Kubo et al., in: Proceedings of ICPP and the 25th EPS Conference on Controlled Fusion and Plasma Physics, Praha, 29 June–3 July 1998, p. 427.